ARTICLE

Check for updates

Targeted artificial ocean cooling to weaken tropical cyclones would be futile

James Hlywiak [1✉] & David S. Nolan[1]

Proposals to use technology to cool sea surface temperatures have received attention for the potential application of weakening a tropical cyclone ahead of landfall. Here, application of an ocean-mixing aware maximum potential intensity theory finds that artificial ocean cooling could drastically weaken tropical cyclones over high sea surface temperature and deep ocean mixed layer environments, especially for fast storm motion speeds. In contrast, realistic mesoscale numerical simulations reveal that massive regions - the largest evaluated here contains a volume of 2.1×10^4 km^3 and a surface area of 2.6×10^5 km^2 - of artificially cooled ocean waters could weaken a tropical cyclone two days before landfall by 15% but only under the most ideal atmospheric and oceanic conditions. Thus, the fundamental theory provides an unreachable upper-bound that cannot be attained even by expending vast resources.

[1] University of Miami Rosenstiel School of Marine, Atmospheric, and Earth Science, Miami, FL 33149, USA. ✉email: jah388@miami.edu

There is great societal interest in reducing the hazards and impacts associated with tropical cyclone (TC) landfalls. Attention is mainly focused on reducing the potential for damage through means such as more accurate forecasts, timely warning and evacuation systems, and more resilient infrastructure. In addition, geoengineering methods - i.e., artificial modification of weather and/or climate - have been commonly proposed to mitigate natural disasters. The term geoengineering encompasses a wide spectrum of applications, including solar radiation management (SRM[1–4]) to mimic a reduction in solar intensity as well as cloud-seeding within the lower-troposphere[5,6]. However, to date, there have been no successful attempts to weaken a TC using geoengineering methods. This is due to myriad factors, including the massive scale of even the smallest TCs, limits in current technology, and warranted trepidation towards unintended consequences.

One of the first efforts to artificially weaken the intensity of a TC was Project STORMFURY[7]. The goal of STORMFURY was to target specific events, rather than a modification of the regional climate on a larger time-scale, and thus is an example of a weather modification strategy. Ultimately, the project was disbanded due to a lack of attributable results. More recently, as the planet continues to warm and humanity reckons with anthropogenic global warming, SRM is an oft-proposed solution for combating increasing concentrations of greenhouse gases through methods such stratospheric aerosol injections (SAI[1,3]). While using SRM to alter the climate is a massive undertaking with potentially even more disastrous results[8,9], studies have suggested that SRM may be an effective tool in mitigating the effects of global warming for select regions of the globe[2,4]. However, such studies note that the benefits may not be spatially uniform, and some regions may experience even worse negative consequences. Thus, even with scientific evidence supporting potential upsides, extensive further research is warranted.

Other studies investigate the impacts of techniques which modify the local regional climate near the surface via lower-tropospheric cloud seeding[5,6] with a number identifying weakening TCs as a possible application[10,11]. Most relevant to this study, artificial cooling of the upper ocean through vertical mixing of cool, sub-thermocline waters as a bottom-up approach has been the motivation behind several recent patent applications in the United States[12–16]. Some of these artificial ocean cooling proposals have been abandoned and none have offered proof of success. Regardless, the idea is still being advanced by privately-funded projects[17].

These efforts are based on taking advantage of the fundamental link between the TC intensity and air-sea fluxes of heat and momentum, as described by the seminal wind-induced surface heat exchange (WISHE[18]) and maximum potential intensity (MPI[19]) theories. Deep layers of warm near-surface waters promote the sustenance of high latent and sensible heat fluxes from the ocean surface, which provide the energy necessary to power a TC. Limited surface heat fluxes is the primary reason for why TCs decay quickly over land[20–23]. Over the ocean, the negative feedback between the TC wind field and sea surface temperatures (SSTs) is one process which naturally dampens the maximum intensity far below what MPI predicts, as cold wakes several degrees Celsius lower than the surrounding waters can develop due to vertical ocean mixing and upwelling of cool water[24–26]. The self-induced cold wake not only reduces intensity, but also weakens the strength and power output of the broader circulation[27]. However, SST cooling via this natural feedback may not be sufficient to limit development of strong TCs when the ocean is characterized by large ocean heat contents[28,29] or inverted vertical temperature gradients[30–32]. Thus, technology could aid in further cooling of the upper-ocean in situations for which the natural wind stress-SST negative feedback is weak, suggesting that technology-aided cooling would be a useful pursuit in these circumstances. However, this line of reasoning is based on a simplified model of TC intensification, and basic intuition suggests that a very large region of ocean waters would have to be cooled for this to be remotely effective. Therefore, assuming this is possible, would targeted artificial cooling have an appreciable effect on an approaching TC?

Here, we address the effectiveness of weakening a TC approaching land using artificial cooling of the upper-ocean. Artificial in this context refers to cooling produced via human intervention. We focus on targeting individual weather events - i.e., weather modification - rather than climate modification. The goal here is not to discuss how technology-aided cooling can be achieved - nor do we consider the potential for unforeseen ecological consequences - but rather to quantify the scales of artificial SST cooling required to produce a noticeable impact on intensity. We use two methods: (1) computation of changes in TC intensity through a modified version of MPI theory which accounts for TC-induced ocean mixing, and (2) through highly realistic, idealized, three-dimensional mesoscale simulations. The first provides a basic framework to asses which environments are the most worthwhile to apply artificial cooling utilizing theory often invoked to support the effectiveness of artificial ocean cooling, while the numerical simulations provide a more realistic assessment of the identified parameter space most likely to benefit from SST cooling. We emphasize the minimum central pressure - P_{min} - and the integrated kinetic energy produced by tropical storm force winds at the 10 m level - IKE_{TS} - as the metrics for TC intensity, as studies have shown that these better correlate to damages than the maximum sustained surface wind speed[33,34].

Results

Artificial cooling within the framework of maximum potential intensity theory. While the original MPI theory does not account for cooling of the SSTs due to the surface wind stress, the ocean-aware potential intensity (OPI) model[35] does by updating the SST within the original framework based on the anticipated cooling due to vertical mixing. Figure 1 reveals the MPI and OPI for atmospheric temperature and moisture vertical profiles characteristic of the Gulf of Mexico in September (see Methods). MPI represents the ocean only through the static SSTs, while the three main parameters we explore in OPI are the initial SSTs, ocean mixed layer depths (MLD), and TC translation speed (i.e., forward motion speed). OPI is generally less than MPI, as self-induced SST cooling limits intensity. All else being equal, OPI increases for increasing base SST, MLD, and translation speed. The physical interpretation is that the deeper the MLD and the lower the residence time of the wind stress over the ocean, the less effective the wind stress is at cooling SSTs.

Figure 2 reveals the increase in P_{min} (i.e., TC weakening) predicted by OPI and MPI if the entire mixed layer is cooled instantaneously by varying amounts down to the MLD. Regimes for which the increase in P_{min} is greatest indicate for what TC and environmental conditions artificial cooling is most effective. The most pronounced results are also those for which OPI predicts the largest maximum intensities; that is, a deeper MLD, greater initial base SST, and faster translation speed. In the scenario of a 60 m deep MLD and translation speed of 4 m s^{-1} - typical of a Gulf of Mexico landfall - OPI predicts the possibility for a weakening of nearly 60 hPa due to mixed layer cooling. Further weakening is predicted if the subsurface water down to 100 m is cooled and for increasing the translation speed. Thus, based on OPI, fast-moving TCs over deep mixed layers would be the ideal cases to employ artifical vertical ocean mixing. Stated another
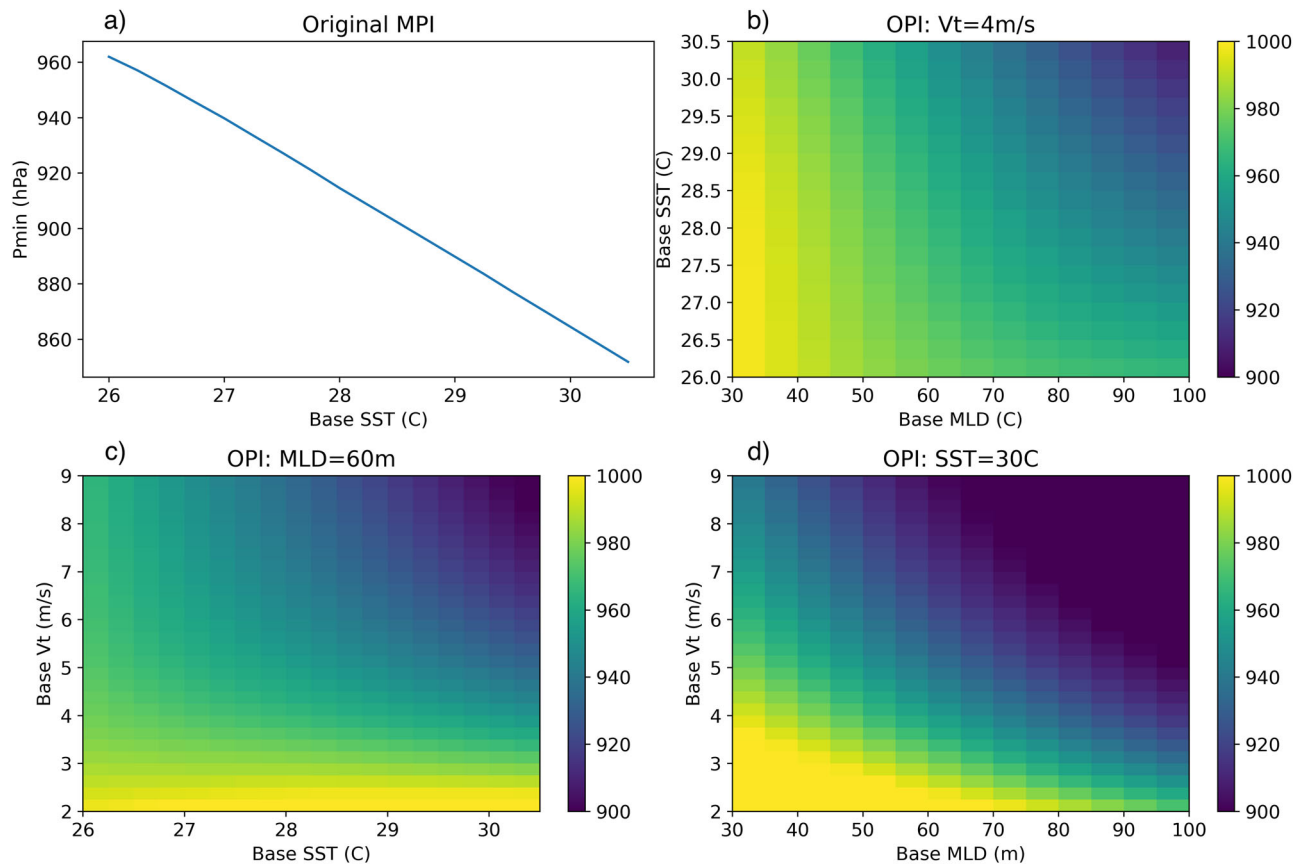
Fig. 1 Maximum potential intensity and ocean-aware potential intensity as functions of SST, MLD, and Vt. a MPI (hPa) as a function of SST, **b** OPI (hPa) as a function of initial SST and MLD for a constant translation speed of 4 m s^{-1}, **c** OPI (hPa) as a function of initial SST and translation speed for a constant MLD of 60 m, and **d** OPI (hPa) as a function of translation speed and MLD for a constant SST of 30 °C.

way, the benefits of artificial cooling are more marginal for slowly translating TCs over thin mixed layers because the TC-induced cooling is already strong in these scenarios.

Artificial cooling within the framework of realistic simulations. MPI and OPI are based on the assumption that the ocean conditions are uniform across an infinite horizontal expanse. In reality, TCs traverse multiple different ocean regimes characterized by varying vertical density profiles and upper-ocean currents. Additionally, our computations presented in Fig. 2 assume an instantaneous introduction of the pre-cooled TC to an artificially cooled region, as opposed to a more realistic gradual exposure of the TC to a cold patch. Thus, the wind stress represented by the maximum surface wind speed included within our computations of OPI likely result in an overestimation of the effects of artificial cooling. To address these assumptions, we performed idealized simulations of TCs making landfall to determine the impact of finite-sized artificially cooled regions on the landfall intensity.

Simulations were performed using the Weather, Research, and Forecasting (WRF) model version 4.2.1. The control simulation - NC, i.e., no cooling - made landfall eight days after initialization. This TC translated at ~4 m s^{-1} due westward. First, three simulations were performed using different sized patches of cooled and deepened mixed layers of varying horizontal widths extending from the coastline. The along-coast length for each was held constant at 720 km while the width from the coastline extended 90, 180, and 360 km from the coastline (see Fig. 3). In addition to these three, a simulation was performed for which the TC encounters a the 90 km wide cool patch earlier. Furthermore,

four additional simulations were performed with identical cool patches but with the TC translating at 8 m s^{-1}. Note that our methods assume the capability to cool a region instantaneously in ocean conditions featuring substantial wind-driven currents.

Figure 4a, b reveals time-series of P_{min} for each simulation. Additionally, Table 1 reveals the precise reduction in intensity at landfall from the lifetime maximum intensity (LMI) for each case, represented by the absolute pressure increase and the percent change relative to the corresponding NC simulation (see Methods). Weakening for each case began a few hours before the center of the TC reached the edge of the cool patch. For the slow simulations, in the absence of artificial cooling, the TC-induced cooling was strong enough to weaken each TC by over 24 hPa in the 12 h before landfall. The largest cool patch weakened the TC an additional 14.4 hPa or 15.2%, however, the change was only 3.5 and 6.4 hPa (3.7 and 6.8%) for W90 and W180. As each TC continued to weaken in time after reaching the cool patch, an additional simulation (W90E; "E" for "earlier") was performed consisting of a 90 km wide cool patch placed away from the coastline - specifically, at the edge of the 360 km patch. This was done to test the possibility of triggering a continuous weakening trend earlier by using a much smaller patch. However, after passing the cool patch, W90E encountered warmer waters and weakening ceased.

The fast simulations resided over each patch for a shorter amount of time, and thus made landfall at higher intensities. Absolute reductions in P_{min} from the LMI were smaller than for the slow simulations, however the reduction percentages relative to the NC Fast simulation were greater. This indicates that although these fast simulations weakened less at landfall, the artificial cooling made up for the lack of TC-induced SST cooling, as suggested by OPI.
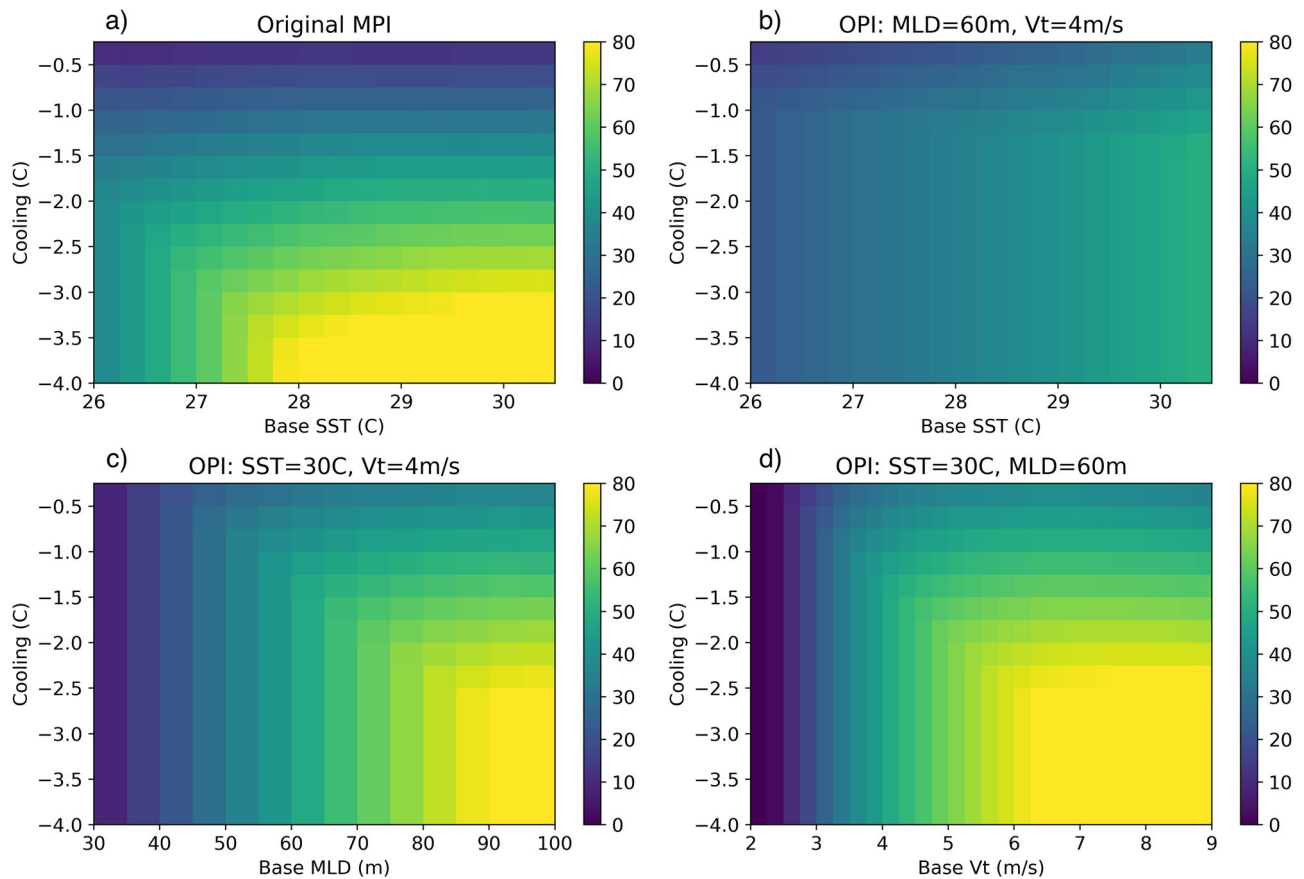
Fig. 2 Weakening of potential intensity after artificial cooling is introduced, as functions of degree of artificial cooling, SST, MLD, and Vt. a Increase in P_{min} predicted by MPI as a function of initial SST and artificial cooling, **b** increase in P_{min} predicted by OPI as a function of initial SST and artificial cooling, **c** increase in P_{min} predicted by OPI as a function of initial MLD and artificial cooling, and **d** increase in P_{min} predicted by OPI as a function of translation speed and artificial cooling.
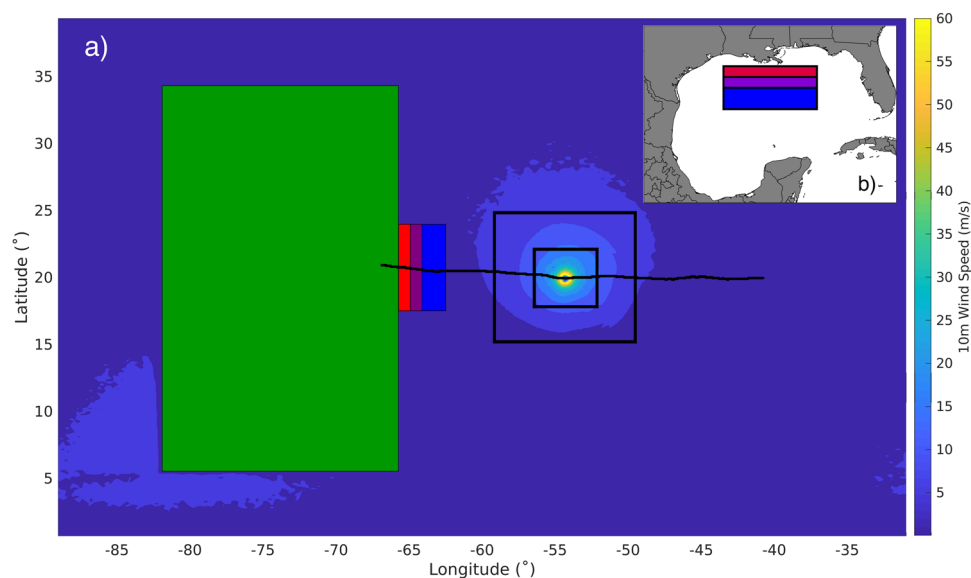

Fig. 3 Simulation domain set-up featuring example schematic of equivalent cool patch sizes for perspective. a Size of the TC wind field at the time of initialization of the sensitivity experiments in relation to each domain, the land mass, the total eight-day track, and each of the three artificially cooled patches. For reference, **b** reveals the size of each patch relative to the Gulf of Mexico.
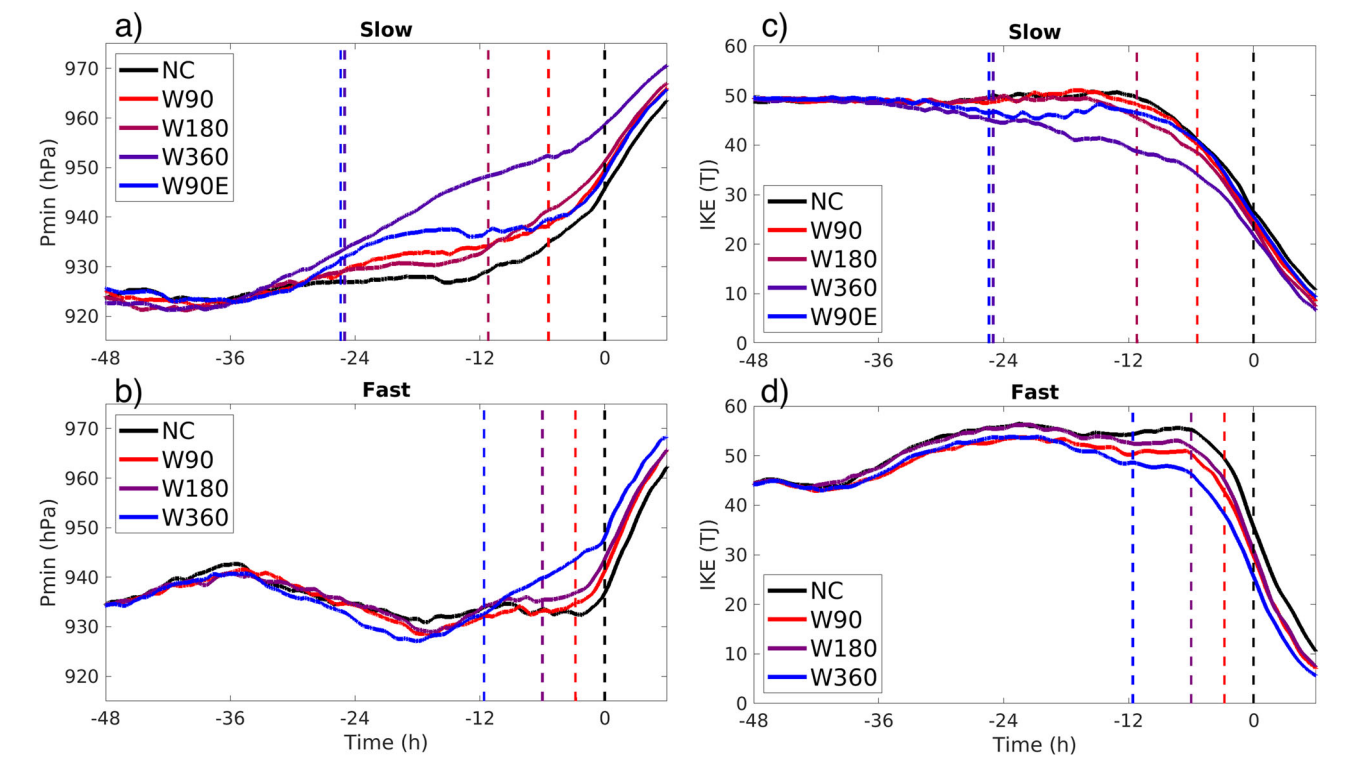
Fig. 4 Time-series of minimum central surface pressure and integrated kinetic energy for all simulations. Time-series of P_{min} for the **a** slow and **b** fast experiments beginning 48 h before landfall. The colored vertical dashed lines indicate the time that the corresponding TC center reached the cool patch boundary, and the black vertical dashed line indicates the time that each TC made landfall. A one-hour running average was applied to each time-series. **c**, **d** As for **a** and **b**, for IKE_{TS} (TJ).

Table 1 Lifetime maximum intensity (LMI, hPa), P_{min} at landfall (hPa), absolute reduction in P_{min} at landfall from the LMI (hPa), and the additional percent reduction relative to the corresponding NC case and normalized by the LMI.

	LMI (hPa)	P_{min} at landfall (hPa)	Reduction from LMI (hPa)	Relative to NC (%)
NC slow	921.6	945.9	24.2	–
W90 slow	921.6	949.3	27.7	3.7
W180 slow	920.4	951.0	30.6	6.8
W360 slow	920.2	958.8	38.6	15.2
W90E slow	922.0	948.5	26.5	2.5
NC fast	929.8	937.3	7.5	–
W90 fast	927.4	940.8	13.4	6.8
W180 fast	928.1	943.4	15.3	9.0
W360 fast	926.5	947.8	21.3	15.6

Table 2 As in Table 1, for IKE_{TS}.

	LMI (TJ)	IKE_{TS} at landfall (TJ)	Absolute reduction (TJ)	Relative to NC (%)
NC slow	51.9	26.6	25.3	–
W90 slow	51.4	24.4	27.0	3.3
W180 slow	51.3	23.6	27.7	4.7
W360 slow	51.4	21.7	29.7	8.6
W90E slow	51.9	25.5	26.5	2.3
NC fast	56.6	35.5	21.1	–
W90 fast	53.8	29.7	24.1	5.6
W180 fast	56.4	30.9	25.5	7.8
W360 fast	53.9	25.5	28.4	13.5

Regardless, W360 Fast required a massive volume of cooled waters for only a 15.6% reduction relative to the NC Fast simulation.

As storm surge is a leading cause for fatalities and damages associated with landfalling TCs, we computed the integrated kinetic energy IKE_{TS} (see methods) for each simulation. When evaluated for surface wind speeds greater than tropical storm strength, IKE_{TS} correlates well with storm surge potential[33]. Results using this metric are shown in Fig. 4c, d and also Table 2. The percent reductions relative to NC are even smaller than when using P_{min}. Additionally, the reduction rate for W90 Slow was a full percentage point greater than for W90E. IKE_{TS} does decrease by ≈5 TJ for W90E relative to W90 a day before landfall, however strengthening ensued once W90E reached warmer waters and weakening stopped, resulting in nearly identical intensities at landfall between W90E and W90.

Discussion

OPI - the modified version of the formative theory relating SSTs to TC intensity - suggests that technology-induced cooling could substantially weaken TCs, especially for greater initial SSTs, MLD, and translation speed - i.e., conditions for which the natural wind-driven cooling feedback is least effective at weakening strong TCs. However, the results from realistic numerical simulations reveal that in practice, artificial cooling would need to be performed on a massive scale to have a meaningful impact on intensities at landfall. Additionally, the scenarios for which technology-induced vertical mixing would most benefit - i.e., for deeper MLD and faster translation speeds - would require an even greater coverage of artificially cooled waters due to the decreased TC residence time over cooled waters. The reductions revealed here are likely overestimates, as experiments were designed under ideal situations. Thus, inducing artificial cooling to substantially weaken the intensity of TCs at landfall would require astronomical efforts to produce noticeable benefits. The amount of
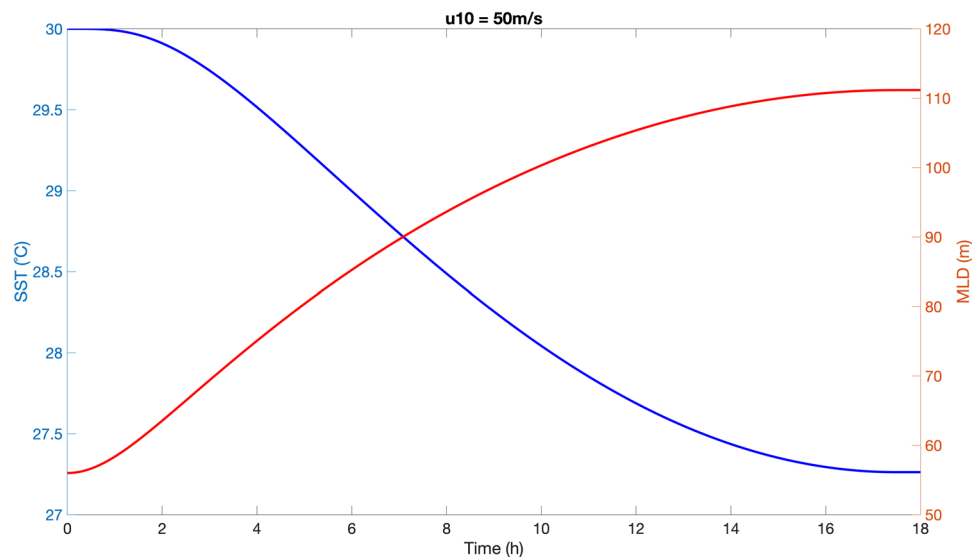
Fig. 5 Time-scales of MLD deepening and SST cooling for a hypothetical constant surface wind forcing as described by the PRT model. PRT solutions for SST - equivalent to the mixed layer temperature - and MLD for a surface wind stress of 50 m s^{-1} as a function of time at 20°N.

ocean heat content extracted from each cool patch within the simulations presented here were 2.8×10^{18}, 1.1×10^{19}, and 4.5×10^{19} kJ, respectively, underscoring the massive quantity of energy that would have to be redistributed. To contextualize these values, back-of-the-envelope calculations reveal that these energy values are roughly equivalent to the amount of energy from the sun that strikes the entire Earth over a period of 10 min. Additionally, the United States Energy Information Administration estimates the total energy consumption across the United States in 2019 alone was roughly 1×10^{17} kJ[36].

A key simplification made in our simulations was an initially quiescent ocean, for which all ocean cooling was a product of the vertical mixing induced by surface wind stresses. In reality, coastal oceans feature strong boundary currents and mesoscale eddies, which shape the upper ocean temperature in complex ways. Warm core eddies often provide boosts to passing TCs[28,37]. Cold core eddies typically produce the opposite effects, however in some cases such features can actually produce horizontal advection patterns that favor intensification[38]. Thus, not only would artificial cooling need to contend with overcoming the natural vertical stability on the order of a hundred meters deep within an eddy but also with strong natural horizontal gradients in temperature and current speed. Also, TCs are a natural component of the planetary climate system and weakening them may result in disastrous side effects. For example, artificial vertical mixing may accelerate upper-ocean deoxygenation[39]. Following this, the biological consequences of artificial SST modification are not well understood and difficult to generalize, and ample caution must be taken to avoid catastrophic ecological habitat changes.

Additionally, we assume ideal atmospheric conditions - that is, temperature and moisture profiles typical of the Gulf of Mexico during the peak of the Atlantic hurricane season in addition to very light vertical wind shear. Natural changes to the mesoscale and synoptic atmospheric patterns could render any technological endeavors pointless, regardless of the oceanic conditions. We also note that our environmental conditions are sampled from just one region. While the exact values of weakening and OPI revealed will depend on the exact ambient characteristics of the environment, we believe our conclusions apply to all ocean basins. Environmental conditions supporting TCs can be generalized across the globe[40], and the fundamental processes occurring at the air-sea interface are, in principal, universal.

Another important caveat to note is that the TCs considered here are in a quasi-steady state. The ocean heat content ahead of a TC is used as a predictor for rapid intensification (RI) within statistical intensity models[41,42], thus one could argue that cooling the ocean ahead of an intensifying TC would be worth considering. However, some studies have suggested that pre-storm SSTs may explain only a small percentage of the variance of intensification, particularly within the Atlantic Basin[43,44]. Consequently, RI is difficult to predict, and discerning for which cases artificial ocean cooling would hinder RI is a tremendously difficult task. Lastly, weaker systems are more prone to sudden shifts in track. Therefore, knowing exactly where to deploy artificial cooling ahead of such systems adds another layer of complexity. Thus, we strongly advise that resources directed towards ineffective geoengineering techniques would be better spent on improved forecasting, more resilient infrastructure, and directed advances in observational technologies.

Methods

Maximum potential intensity calculations. MPI calculations were performed using the PyPI Python package[45,46]. Vertical profiles of atmospheric temperature and mixing ratio were provided by ERA5 monthly-averaged soundings from the Gulf of Mexico in September, averaged between the years 2010–2020[47]. The original PyPI code was modified by the authors to utilize OPI based on the equations from Miyamoto et al.[35]. The procedure to compute OPI here is as follows: first, the standard MPI is computed. The maximum potential winds were obtained from this first computation and along with a prescribed initial MLD and translation speed were input into the SST update equation - eq 10 of Miyamoto et al.[35]. For simplicity, we prescribed the drag coefficient $C_d = 2.5 \times 10^{-3}$, size parameter $\Lambda = 66.33$ km, and initial temperature discontinuity at the base of the mixed layer $\Delta T = 0$. Offline tests revealed little sensitivity of the results to changes in these parameters. Finally, the original MPI was once again computed using the updated SST to obtain OPI. This value for OPI/MPI was used as the base state. To compute the change in OPI due to artificial cooling, OPI was once again computed from the OPI and SST values of the base state, where the base SST was reduced by a range of cooling values from 0.25 to 4 °C.

Numerical simulation procedures. All simulations were performed using the advanced-research WRF (WRF-ARW) core version 4.2.1. The control simulation was initialized as a weak vortex ($P_{min0} \approx 1005$ mb) embedded within a mean easterly flow by the point-downscaling (PDS) method[48]. The vertical temperature and moisture profiles were the same as those used for the OPI calculations, i.e., ERA5 monthly-averaged soundings from the Gulf of Mexico in September averaged between the years 2010–2020[47]. Note that although these soundings were taken over the Gulf of Mexico, they represent generic soundings conducive for TC development within any tropical region. The wind speed below 850 hPa was prescribed at 5 m s^{-1}, decreasing sinusoidally to 2.5 m s^{-1} above 200 hPa resulting in

bulk westerly vertical wind shear of 2.5 m s^{-1}. Three domains were enabled, with the inner two following the vortex as it moved. Horizontal resolutions were δx, $\delta y = 18, 6$, and 2 km spanning 360×240, 180×180, and 240×240 grid points in the zonal and meridional directions, respectively. The parent domain was doubly-periodic and set on an f-plane corresponding to the Coriolis parameter at 20°N. Large-scale nudging was applied to the parent domain using the time-varying PDS (TVPDS) method[49], for which the nudging interval and nudging time scale were 24 h and $\tau = 12$ h, respectively. The WRF single-moment 5-class[50] microphysics option was enabled and convection was parameterized for the outermost domain using the modified Tiedtke scheme[51]. Incoming solar and outgoing long-wave radiation schemes were disabled to remove diurnal influences. The Mellor–Yamada–Janjic (MYJ) planetary boundary layer scheme was enabled along with the MYJ-modified surface layer scheme within WRF[52], and the surface drag coefficient saturates at high wind speeds[53].

A large land mass was initialized within the control simulation using the Noah Land Surface model[54] as seen in Fig. 3. The land mass featured loam soil characteristics, and the roughness length and soil moisture contents were static at $z_0 = 25$ cm and $S_c = 0.3$, respectively. Land temperatures were static in time and space at 27 °C. The control simulation made landfall roughly seven and a half days into the simulation, which ended after eight days. After four days of forward integration, the control set was paused and variables stored. All sensitivity simulations proceeded from this state over the remaining four days. For the fast set of simulations, TVPDS was used to accelerate the background steering flow over the course of the following day after restart towards 10 m s^{-1} below 800 hPa and 7.5 m s^{-1} above 200 hPa, thus maintaining 2.5 m s^{-1} of vertical westerly shear.

In all cases, the ocean was represented by the standard 1D ocean mixing model available within WRF[55], for which MLD$_0 = 50$ m and the lapse rate below was prescribed to $\Gamma = 0.1$ K m^{-1}. Bathymetry was not smoothed to meet the surface at the coastline, as the bottom boundary is treated as infinitely deep. Changes in vertical salinity were not considered. For the artificial cooling simulations, the mixed layer temperature was cooled by $\Delta T = 2$ °C from the initial 30 °C, and the MLD was deepened from roughly 58 m to ~80 m to avoid instabilities in the vertical temperature profile. We chose 2 °C based on Fig. 2b, which reveals that cooling beyond this threshold results in minimal further reductions of OPI. We also presume that the forecasted landfall point is perfect three days in advance. The volumes of the W90, W180, and W360 cool patches were thus ~5.1×10^3, 1.0×10^4, and 2.1×10^4 km^3. Note that the deepening and cooling here mimics a sudden removal of the heat from the upper ocean and does not reflect the amount of mixing actually needed to cool the column via entrainment mixing from below, a popular cooling method proposed in several of the aforementioned patents. We elect to cool the ocean in this way to remain agnostic towards the method for heat removal. To evaluate how this compares to the wind-driven cooling via vertical mixing from a typical TC, Fig. 5 reveals solutions of SST and MLD from the PRT model. For a 50 m s^{-1} surface wind stress and 58 m initial MLD, SST cooling of $\Delta T = 2$ °C would occur after roughly 10 h, while a deepening of the MLD from 58 to 80 m would occur after roughly 5 h, compared to the instantaneous cooling and deepening employed within the WRF simulations. One notable difference to the total vertical ocean profile between non-conserved heat removal and cooling via vertical mixing is that mixing warms the waters beneath the thermocline whereas the former retains the original composition of the vertical profile. Thus, the ensuing TC-induced cold-wake following mixing would theoretically be less effective compared to the heat removal method.

Computation of intensity metrics. In Table 1, the percent reduction relative to the control case was calculated by first taking the difference in reduction from LMI - the third column - between each cooling case and the control case. Then, this value was normalized by the LMI of each cooling case, which was represented by the environmental pressure deficit - i.e., $1015 - P_{min}$. The equivalent metric for IKE_{TS} was normalized by the absolute LMI, i.e., the first column.

IKE_{TS} was computed using (1). IKE_{TS} is the area-integrated kinetic energy at the 10 m level, where U_{10} is the wind field at 10 m and the density ρ is assumed to be 1 kg m^{-3}. The area integral is only computed over the area with winds above tropical storm strength on the Saffir-Simpson Wind Scale (18 m s^{-1}) as storm surge and wave generation scale with the kinetic energy output above this threshold. The integral is multiplied by a vertical depth of 1 m to yield units of energy in Joules.

$$IKE_{TS} = \frac{1}{2}\rho \int_A U_{10} dA \qquad (1)$$

Data availability
ERA5 monthly sounding data from over the Gulf of Mexico can be found at https://cds.climate.copernicus.eu.

Code availability
The PyPI MPI code can be found at https://github.com/dgilford/tcpyPI. Contact J.H. for access to the OPI Python codes.

References
1. Moore, J. C. et al. Atlantic hurricane surge response to geoengineering. *Proc. Natl Acad. Sci. USA* **112**, 13794–13799 (2015).
2. Jones, A. C. et al. Impacts of hemispheric solar geoengineering on tropical cyclone frequency. Nat. Commun. **8**, https://doi.org/10.1038/s41467-017-01606-0 (2017).
3. Jones, A. C. et al. Regional climate impacts of stabilizing global warming at 1.5 K using solar geoengineering. *Earth Future* **6**, 230–251 (2018).
4. Irvine, P. et al. Halving warming with idealized solar geoengineering moderates key climate hazards. *Nat. Climate Change* **9**, 295–299 (2019).
5. Latham, J. et al. Marine cloud brightening. *Philos. Trans. R. Soc. A* **370**, 4217–4262 (2012).
6. Ahlm, L. et al. Marine cloud brightening - as effective without clouds. *Atmos. Chem. Phys.* **17**, 13071–13087 (2017).
7. Willoughby, H. E., Jorgensen, D. P., Black, R. A. & Rosenthal, S. L. Project STORMFURY: a scientific chronicle 1962-1983. *Bull. Am. Meteorol. Soc.* **66**, 505–514 (1985).
8. Robock, A., Bunzl, M., Kravitz, B. & Stenchikov, G. L. A test for geoengineering? *Science* **327**, 530–531 (2010).
9. Robock, A., MacMartin, D. G., Duren, R. & Christensen, M. W. Studying geoengineering with natural and anthropogenic analogs. *Clim. Change* **121**, 445–458 (2013).
10. Latham, J. et al. Marine cloud brightening: regional applications. *Philos. Trans. R. Soc. A* **372** 1–11 (2014).
11. MacCracken, M. C. The rationale for accelerating regionally focused climate intervention research. *Earth Future* **4**, 649–657 (2016).
12. Uram, H. United States Patent Application Publication No. 0008155A1. https://patents.google.com/patent/US20020008155A1/en?inventor=herbert+uram&oq=herbert+uram (2002).
13. Kitamura, K. United States Patent Application Publication No. 7832657B2. https://patents.google.com/patent/US7832657B2/en?oq=7%2C832%2C657 (2010).
14. Gradle, R. United States Patent Application Publication No. 8148840B2. https://patents.google.com/patent/US7832657B2/en?oq=7%2C832%2C657 (2012).
15. Tawil, J. J. United States Patent Application Publication No. 0038063A1. https://patents.google.com/patent/US20130038063A1/en?assignee=jack+joseph+tawil&oq=jack+joseph+tawil (2013).
16. Bowers, J. A. et al. United States Patent Application Publication No. 8685254B2. https://patents.google.com/patent/US8685254B2/en?oq=8685254 (2014).
17. OceanTherm: https://www.oceantherm.no/ (2021).
18. Emanuel, K. A. An air-sea interaction theory for tropical cyclones. Part I: steady-state maintenance. *J. Atmos. Sci.* **43**, 585–605 (1986).
19. Emanuel, K. A. The maximum intensity of hurricanes. *J. Atmos. Sci.* **45**, 1143–1155 (1988).
20. Miller, B. I. A study of the filling of Hurricane Donna (1960) over land. *Mon. Weather Rev.* **92**, 389–406 (1964).
21. Tuleya, R. E. Tropical storm development and decay: sensitivity to surface boundary conditions. *Mon. Weather Rev.* **122**, 291–304 (1994).
22. DeMaria, M., Mainelli, M., Shay, L. K., Knaff, J. A. & Kaplan, J. Further improvements to the Statistical Hurricane Intensity Prediction Scheme (SHIPS). *Weather Forecast.* **20**, 531–543 (2005).
23. Hlywiak, J. & Nolan, D. S. The response of the near-surface tropical cyclone wind field to inland surface roughness length and soil moisture content during and after landfall. *J. Atmos. Sci.* **78**, 983–1000 (2021).
24. Cione, J. J. & Uhlhorn, E. W. Sea surface temperature variability in hurricanes: implications with respect to intensity change. *Mon. Weather Rev.* **131**, 1783–1796 (2003).
25. D'Asaro, E. A., Sanford, T. B., Niiler, P. P. & Terrill, E. J. Cold wake of Hurricane Frances. *Geophys. Res. Lett.* **34**, 2–7 (2007).
26. Chen, S., Elsberry, R. L. & Harr, P. A. Modeling interaction of a tropical cyclone with its cold wake. *J. Atmos. Sci.* **74**, 3981–4001 (2017).
27. Guo, T., Sun, Y., Liu, L. & Zhong, Z. The impact of storm-induced SST cooling on storm size and destructiveness: results from atmosphere-ocean coupled simulations. *J. Meteorol. Res.* **34**, 1068–1081 (2020).
28. Shay, L. K., Goni, G. J. & Black, P. G. Effects of a warm oceanic feature on Hurricane Opal. *Mon. Weather Rev.* **128**, 1366–1383 (2000).
29. Mainelli, M. M., DeMaria, M., Shay, L. K. & Goni, G. Application of oceanic heat content estimation to operational forecasting of recent Atlantic category 5 hurricanes. *Weather Forecast.* **23**, 3–16 (2008).

30. Balaguru, K. et al. Ocean barrier layers' effect on tropical cyclone intensification. *Proc. Natl Acad. Sci. USA* **109**, 14343–14347 (2012).

31. Hlywiak, J. & Nolan, D. The influence of oceanic barrier layers on tropical cyclone intensity as determined through idealized, coupled numerical simulations. *J. Phys. Oceanogr.* **49**, 1723–1745 (2019).

32. Rudzin, J. E., Shay, L. K. & Cruz, B. J. D. L. The impact of the Amazon-Orinoco River plume on enthalpy flux and air-sea interaction within caribbean sea tropical cyclones. *Mon. Weather Rev.* **147**, 931–950 (2019).

33. Powell, M. & Reinhold, T. Tropical cyclone destructive potential by integrated kinetic energy. *Bull. Am. Meteorol. Soc.* **88**, 513–526 (2007).

34. Klotzbach, P. J. et al. Surface pressure a more skillful predictor of normalized hurricane damage than maximum sustained wind. *Bull. Am. Meteorol. Soc.* **101**, E830–E846 (2020).

35. Miyamoto, Y., Bryan, G. H. & Rotunno, R. An analytical model of maximum potential intensity for tropical cyclones incorporating the effect of ocean mixing. *Geophys. Res. Lett.* **44**, 5826–5835 (2017).

36. U.S. Energy Information Administration. *April 2022 monthly energy review*. Technical Report 4 (U.S. Energy Information Administration, 2022).

37. Ma, Z., Fei, J., Liu, L., Huang, X. & Li, Y. An investigation of the influences of mesoscale ocean eddies on tropical cyclone intensities. *Mon. Weather Rev.* **145**, 1181–1201 (2017).

38. Yablonsky, R. M. & Ginis, I. Impact of a warm ocean Eddy's circulation on hurricane-induced sea surface cooling with implications for hurricane intensity. *Mon. Weather Rev.* **141**, 997–1021 (2013).

39. Feng, E. Y., Su, B. & Oschlies, A. Geoengineered ocean vertical water exchange can accelerate global deoxygenation. *Geophys. Res. Lett.* **47**, e2020GL088263 (2020).

40. Gray, W. M. Global view of the origin of tropical disturbances and storms. *Mon. Weather Rev.* **96**, 669–700 (1968).

41. DeMaria, M., Mainelli, M., Shay, L. K., Knaff, J. A. & Kaplan, J. Further improvements to the Statistical Hurricane Intensity Prediction Scheme (SHIPS). *Weather Forecast.* **20**, 531–543 (2005).

42. Kaplan, J. et al. Evaluating environmental impacts on tropical cyclone rapid intensification predictability utilizing statistical models. *Weather Forecast.* **30**, 1374–1396 (2015).

43. Foltz, G. R., Balaguru, K. & Hagos, S. Interbasin differences in the relationship between SST and tropical cyclone intensification. *Mon. Weather Rev.* **146**, 853–870(2018).

44. Wadler, J. B., Zhang, J. A., Rogers, R. F., Jaimes, B. & Shay, L. K. The rapid intensification of Hurricane Michael (2018): Storm structure and the relationship to environmental and air-sea interactions. *Mon. Weather Rev.* **149**, 245–267 (2021).

45. Gilford, D. dgilford/pyPI: pyPI v1.3 (initial package release). https://zenodo.org/record/3985975 (2020).

46. Gilford, D. M. PyPI (v1.3): tropical cyclone potential intensity calculations in python. *Geosci. Model Dev.* **14**, 2351–2369 (2021).

47. Hersbach, H. et al. ERA5 monthly averaged data on pressure levels from 1979 to present. Copernicus Climate Change Service (C3S) Climate Data Store (CDS). https://doi.org/10.24381/cds.6860a573 (2019).

48. Nolan, D. S. Evaluating environmental favorableness for tropical cyclone development with the method of point-downscaling. *J. Adv. Model. Earth Syst.* **3**, 1–28 (2011).

49. Onderlinde, M. J. & Nolan, D. S. The tropical cyclone response to changing wind shear using the method of time-varying point-downscaling. *J. Adv. Model. Earth Syst.* **9**, 908–931 (2017).

50. Lim, J. O. J. & Hong, S. Y. Effects of bulk ice microphysics on the simulated monsoonal precipitation over east Asia. *J. Geophys. Res. Atmos.* **110**, 1–16 (2005).

51. Zhang, C., Wang, Y. & Hamilton, K. Improved representation of boundary layer clouds over the southeast pacific in ARW-WRF using a modified tiedtke cumulus parameterization scheme. *Mon. Weather Rev.* **139**, 3489–3513 (2011).

52. Janjic, Z. Nonsingular implementation of the Mellor-Yamada Level 2.5 scheme in the NCEP Meso model. *NCEP Office Note* **437**, 61 (2002).

53. Edson, J. B. et al. On the exchange of momentum over the open ocean. *J. Phys. Oceanogr.* **43**, 1589–1610 (2013).

54. Chen, F. & Dudhia, J. Coupling an advanced Land Surface-Hydrology Model with the Penn State-NCAR MM5 modeling system. Part I: model implementation and sensitivity. *Mon. Weather Rev.* **129**, 569–585 (2001).

55. Pollard, R. T., Rhines, P. B. & Thompson, R. O. The deepening of the wind-mixed layer. *Geophys. Astrophys. Fluid Dyn.* **4**, 381–404 (1972).

Author contributions
J.H. did the majority of the planning and execution of the methods and wrote the majority of the manuscript. D.S.N. conceived the idea for this study. Both J.H. and D.S.N. analyzed the results and edited the manuscript. All simulations and analysis were completed while J.H. was a Ph.D. candidate at the University of Miami.

Competing interests
The authors declare no competing interests.

Additional information
Supplementary information The online version contains supplementary material available at https://doi.org/10.1038/s43247-022-00519-1.

Correspondence and requests for materials should be addressed to James Hlywiak.

Peer review information *Communications Earth Environment* thanks the anonymous reviewers for their contribution to the peer review of this work. Primary Handling Editors: Viviane Menezes, Joe Aslin, Heike Langenberg. Peer reviewer reports are available.

Reprints and permission information is available at http://www.nature.com/reprints

Publisher's note Springer Nature remains neutral with regard to jurisdictional claims in published maps and institutional affiliations.